2011

Investigation of Singlemode-Multimode-Singlemode and Singlemode-Tapered Multitmode-Singlemode Fibre Structures and Their Application for Refractive Index Sensing

Pengfei Wang
Technological University Dublin, pengfei.wang@tudublin.ie

Gilberto Brambilla
University of Southampton

Ming Ding
University of Southampton

See next page for additional authors

Recommended Citation

Wang, P., Brambilla, G.,Ding, M., Semenova, Y., Wu, Q., Farrell, G.:Investigation of singlemode-multimode-singlemode and singlemode-tapered multimode-singlemode fibre structures and their application for refractive index sensing. Journal of the Optical Society of America B, Vol.28, 5, 2011, pp. 1180-1186. doi:10.1364/JOSAB.28.001180

Investigation of single-mode–multimode–single-mode and single-mode–tapered-multimode–single-mode fiber structures and their application for refractive index sensing

Pengfei Wang,[1,2,*] Gilberto Brambilla,[1] Ming Ding,[1] Yuliya Semenova,[2] Qiang Wu,[2] and Gerald Farrell[2]

[1]*Optoelectronics Research Centre, University of Southampton, Southampton SO17 1BJ, UK*
[2]*Photonic Research Centre, Dublin Institute of Technology, Kevin Street, Dublin 8, Ireland*
**Corresponding author: pw3y09@orc.soton.ac.uk*

Received January 11, 2011; revised February 28, 2011; accepted March 7, 2011;
posted March 16, 2011 (Doc. ID 140933); published April 19, 2011

All-fiber in-line single-mode–multimode–single-mode (SMS) and single-mode–tapered-multimode–single-mode (STMS) fiber structures are investigated. A wide-angle beam propagation method in cylindrical coordinates is developed and employed for numerical simulations of the light propagation performance of such fiber devices. The effect of strong mode interference on the performance of the devices is studied and verified numerically; results indicate that the proposed STMS structure can be exploited for measuring a broad refractive index range with reasonable high resolution, compared with the conventional SMS structure. © 2011 Optical Society of America

OCIS codes: 060.2310, 060.2340, 060.2370.

1. INTRODUCTION

Recently, the multimode interference occurring in the single-mode–multimode–single-mode (SMS) fiber structure has been investigated and proposed as a basis for a number of novel fiber devices [1–4]. Optical devices based on SMS fiber structures offer all-fiber solutions for optical communications and optical sensing with the advantages of ease of packaging and interconnection to other fiber optic components. Using the dependence of the device transmissivity on the refractive index of the surrounding environment, the authors in [3] have demonstrated a refractometric sensor for several lengths of the multimode fiber (MMF) section of an SMS structure. However, the dynamic range (measurable refractive index range) of such a fiber refractometer is limited by the refractive index value of the MMF core. In order to extend the sensor dynamic range without increasing the difficulty and the cost of fabrication, this paper reports, for the first time to our knowledge, the use of a tapered MMF sandwiched between two single-mode fibers (SMF) as a refractometric sensor, henceforth referred to as a single-mode–tapered multimode–single-mode (STMS) structure.

Accurate theoretical modeling and simulation of light behaviors are essential in developing these SMS-based optical fiber devices. Conventionally, numerical simulation, such as mode propagation analysis (MPA) is popular in use for substantiating and validating the experimental results of straight and uniform structures of SMS, due to its simplicity. However, for some other types of SMS-based fiber devices, such as bent SMS or tapered SMS structures, simulations based on a three-dimensional model are preferred, because existing MPA methods cannot predict accurately such mode conversion and mode interference phenomena in the nonuniform SMS structures. Therefore, in this paper, we present a comprehensive numerical analysis for characterizing the optical properties of both SMS- and STMS-based refractometric sensors. A wide-angle beam propagation method (WABPM) in cylindrical coordinates using the Padé $(3,3)$ approximate operator [5] and perfectly matched layer (PML) boundary conditions has been proposed to numerically analyze the light propagation and sensing performance.

Section 2 presents a brief investigation of the guided-mode propagation within the SMS structure and of its related light transmission; the appropriate lengths of the MMF section are also analyzed for an application as a refractometric sensor.

Section 3 presents a theoretical investigation for an STMS structure using the WABPM model, from which the transmission spectra of the STMS can be easily predicted. Simulations indicate that the STMS structure can act as a refractometer with a broader measurable refractive index range than that of an SMS structure.

Conclusions are presented in Section 4.

2. THEORETICAL MODELING OF LIGHT PROPAGATION IN THE SMS STRUCTURE

A. Proposed SMS configuration and Its Application for Refractive Index Sensing

An SMS fiber structure consists of input and output single-mode fibers with a short section of multimode fiber sandwiched between them, as shown in Fig. 1. For the purpose of refractive index sensing, the multimode fiber cladding is removed by chemical etching. When the core of the multimode fiber section is immersed in a liquid (Fig. 2) this acts as the MMF cladding, and its refractive index influences the light propagation in the multimode section and thus the transmitted light intensity at the MMF–SMF joint.

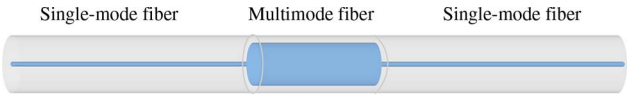

Fig. 1. (Color online) Schematic configuration of the SMS structure.

This SMS fiber refractometer exploits the multimode interference occurring in the MMF section, which depends on the refractive index of the surrounding liquid medium. When the light field propagating along the input SMF enters the MMF section, the input field can be decomposed into the MMF eigenmodes (LP_{nm}). The MMF high-order eigenmodes are excited, and interference between different modes occurs while the beam propagates along the MMF section. At the MMF–SMF join, light is then coupled into the output SMF. With an appropriate design of the SMS structure, the transmission loss of SMS may become a function of the surrounding liquid refractive index; thus by measuring the changes in the transmission loss and assuming a suitable calibration, the refractive index of the surrounding liquid can be determined. In order to optimize the design of the SMS refractometric sensor, a WABPM in a cylindrical coordinate system is employed to simulate light propagation in the multimode fiber section. A brief description of the theoretical model based on the WABPM is presented below.

B. Cylindrical Wide-Angle Beam Propagation Method

It is well known that a scalar wave equation for a symmetric structure in cylindrical coordinates can be expressed as follows:

$$\frac{\partial^2 E}{\partial z^2}+\frac{\partial^2 E}{\partial r^2}+\frac{1}{r}\frac{\partial E}{\partial r}+k^2n^2(r,z)E=0, \tag{1}$$

where k is the wave number in free space and $n(r,z)$ is the refractive index distribution. We assume a slowly varying envelope approximation for the beam propagation method, such as $E(r,z)=\hat{E}(r,z)\exp(jkn_0z)$, where n_0 is the reference refractive index. For $\hat{E}(r,z)$, the corresponding beam propagation equation can be derived as follows:

$$\frac{\partial \hat{E}}{\partial z}=\frac{\frac{j}{2kn_0}P\hat{E}}{1-\frac{j}{2kn_0}\frac{\partial \hat{E}}{\partial z}}, \tag{2}$$

where $P\hat{E}=\left[\frac{\partial^2\hat{E}}{\partial r^2}+\frac{1}{r}\frac{\partial\hat{E}}{\partial r}+k^2(n^2(r,z)-n_0^2)\hat{E}\right]$. With the Padé approximation [5], a Crank–Nicolson finite-difference scheme and multistep method as developed in [6,7], Eq. (2) can be rewritten as

$$\hat{E}^{l+1}=\frac{(1+a_nP)(1+a_{n-1}P)\ldots(1+a_1P)}{(1+a_n^*P)(1+a_{n-1}^*P)\ldots(1+a_1^*P)}\hat{E}^l, \tag{3}$$

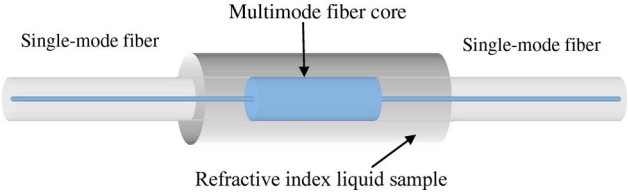

Fig. 2. (Color online) Configuration of the SMS fiber-based refractometer.

where a_i and a_i^* $(i=1,2,\ldots n)$ are determined by the polynomials based on the Padé approximation. Therefore, for the ith step, $\hat{E}^{l+\frac{i}{n}}$ can be solved by

$$\begin{aligned}&a_i^*\eta_-E_{m-1}^{l+\frac{i}{n}}+[1+a_i^*\varsigma]E_m^{l+\frac{i}{n}}+a_i^*\eta_+E_{m+1}^{l+\frac{i}{n}}\\&\quad=a_i\eta_-E_{m-1}^{l+\frac{i-1}{n}}+[1+a_i\varsigma]E_{m-1}^{l+\frac{i-1}{n}}+a_i\eta_+E_{m+1}^{l+\frac{i-1}{n}},\end{aligned} \tag{4}$$

where $\eta_\pm=\frac{1}{\Delta r^2}\pm\frac{1}{2r\Delta r}$ and $\varsigma=\left(k^2(n^2-n_0^2)-\frac{2}{\Delta r^2}\right)$. At the fiber axis,$r=0$, therefore, the L'Hôpital rule can be applied and Eq. (5) can be derived further as follows:

$$\begin{aligned}&\left[1+a_i^*\left(k^2(n^2-n_0^2)-\frac{4}{\Delta r^2}\right)\right]E_0^{l+\frac{i}{n}}+a_i^*\frac{4}{\Delta r^2}E_1^{l+\frac{i}{n}}\\&\quad=\left[1+a_i\left(k^2(n^2-n_0^2)-\frac{4}{\Delta r^2}\right)\right]E_0^{l+\frac{i-1}{n}}+a_i\left[\frac{4}{\Delta r^2}\right]E_1^{l+\frac{i-1}{n}}.\end{aligned} \tag{5}$$

In the practical numerical implementation of the WABPM model, because of the circular symmetry of the proposed fiber structure, it is sufficient to consider only a half-plane, for example, $0\le r\le R$, as the computational region. The PML is employed as the boundary condition of the computational region $(r=R)$.

To calculate the coupling loss of the light field $E(r,z)$ at a propagation distance z from the output SMF, the overlap integration between the light field $E(r,z)$ and the eigenmode of the SMF can be used to save computational time:

$$L_s(z)=10\log_{10}\left(\frac{\left|\int_0^\infty E(r,z)f(r)r\mathrm{d}r\right|^2}{\int_0^\infty|E(r,z)|^2r\mathrm{d}r\int_0^\infty|f(r)|^2r\mathrm{d}r}\right), \tag{6}$$

where $f(r)$ is the fundamental mode of the SMF. It is assumed that the output SMF has the same fiber parameters as the input fiber, $f(r)=E(r,0)$.

C. Optimal Design of the SMS Fiber-Based Refractometer

As a numerical example, light propagation in the multimode fiber section is simulated as follows. The eigenmode of the standard single-mode fiber (Corning SMF28, Corning, Incorporated, USA) at a wavelength of 1550 nm is used as the input field. The parameters used in the model for the MMF section are based on the Thorlabs AFS105/125Y step index MMF (Thorlabs, USA): the core and cladding diameters and refractive indices are 105 μm, 125 μm, $n_{co}=1.4446$ and $n_{cl}=1.4271$, respectively. The refractive index of the surrounding liquid at 1550 nm is assumed to be $n_{ethanol}=1.354$. Figures 3 and 4 present the amplitude distributions of the propagating optical fields and the corresponding transmission loss to the output SMF as a function of the propagation distance for the device in air and in ethanol. It is well known that a single-mode fiber has a circular symmetric characteristic for the fundamental mode, so the input light launched from the single-mode fiber is assumed to have a field distribution of $E(r,0)$, as mentioned above. When the light enters the multimode fiber, the input field will be decomposed into the eigenmodes LP_{nm} of the multimode fiber. Because of the circular symmetric characteristic of the input field, and assuming an ideal axial alignment

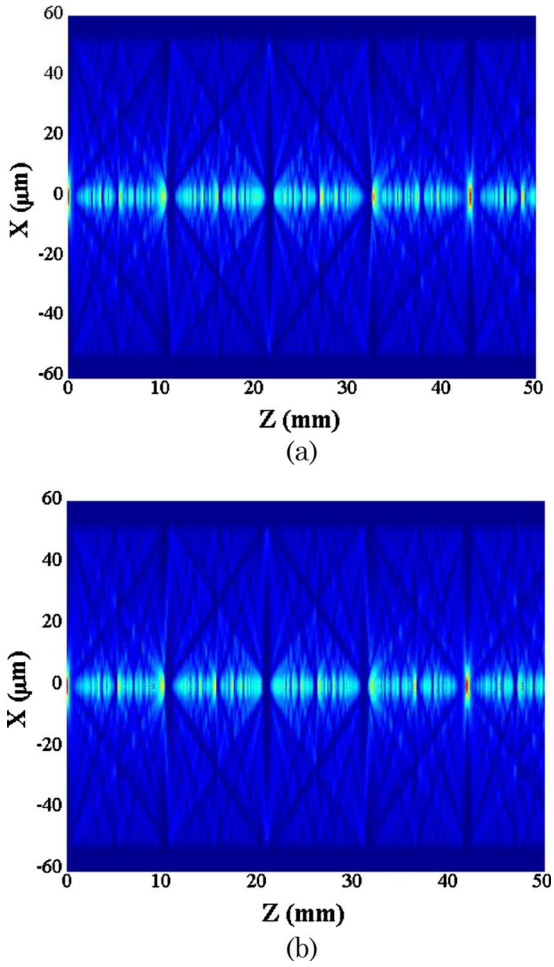

Fig. 3. Amplitude distribution of the propagating light field as a function of propagation distance with an MMF length of 50 mm when the cladding refractive index is (a) $n_{\mathrm{cl}} = 1.4271$, and (b) $n_{\mathrm{ethanol}} = 1.354$, respectively, and the operating wavelength is 1550 nm.

between the core of the single-mode fiber and the core of the multimode fiber, only the LP_{0m} modes can be excited within the multimode fiber section, which has been also addressed in [8]. Denoting the field profile of LP_{0m} as $\psi_m(r)$, the eigenmodes of the multimode fiber are normalized as

$$\int_0^{\infty} |E(r,0)|^2 r\mathrm{d}r = \int_0^{\infty} |\psi_m(r)|^2 r\mathrm{d}r, \qquad m = 1, 2, \ldots, \quad (7)$$

and, neglecting the very small amount of radiation escaping from the interface between the air and the cladding of the multimode fiber, finally we have

$$E(r,0) = \sum_{m=1}^{M} c_m \psi_m(r), \quad (8)$$

where c_m is the excitation coefficient of each eigenmode, and it can be expressed by the overlap integral between $E(r,0)$ and $\psi_m(r)$, as follows:

$$c_m = \frac{\int_0^{\infty} E(r,0)\psi_m(r) r\mathrm{d}r}{\int_0^{\infty} \psi_m(r)\psi_m(r) r\mathrm{d}r}. \quad (9)$$

The excited mode number of the LP_{0m} multimode fiber, $M \approx V/\pi$, (where V is the well-known normalized frequency and a is the radius of the multimode fiber core, n_{co} and n_{cl} are refractive indices of the core and cladding of the multimode fiber, respectively, and λ is the wavelength in the free-space). As the light propagates in the multimode fiber section, the modal interference field at a propagation distance, Z, from the input can be calculated [8] as

$$E(r,z) = \sum_{m=1}^{M} c_m \psi_m(r) \exp(i\beta_m z), \quad (10)$$

where β_m is the propagation constant of each eigenmode propagating within the multimode fiber. Thus the modal interference generated in the MMF section is shown in a dynamic form in Fig. 5 (Media 1), as it evolves along the length of the MMF section.

A useful basis for visualizing and gaining a better understanding of SMS fiber structures is the phenomenon of self-imaging [8]. Self-imaging can be defined as a property

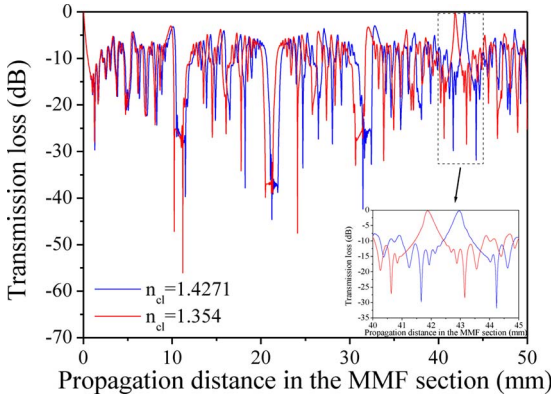

Fig. 4. (Color online) Calculated transmission loss to the output SMF fiber as a function of propagation distance with an MMF length of 50 mm when the cladding refractive index is $n_{\mathrm{cl}} = 1.4271$ (blue curve), and $n_{\mathrm{ethanol}} = 1.354$ (red curve), the operating wavelength is 1550 nm. Inset: a zoomed region in around the propagation distance of 40–45 mm of the MMF section, which shows the details of the shifts of the self-imaging positions due to the change of the cladding refractive index.

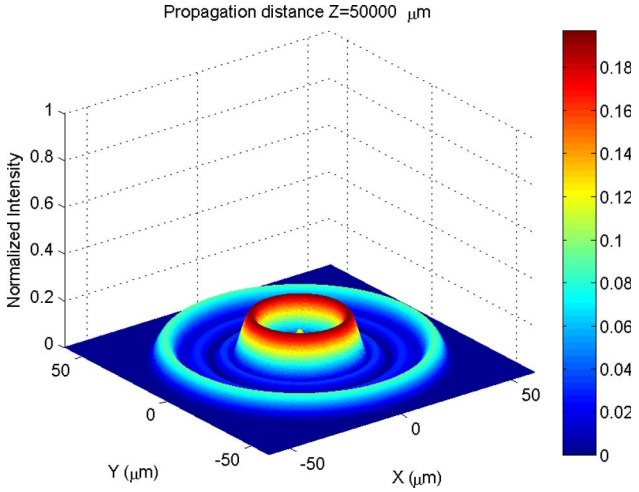

Fig. 5. (Color online) (Media 1) Video of mode interference within the MMF fiber section when the refractive index of the cladding is $n_{\mathrm{cl}} = 1.4271$ at a wavelength of 1550 nm, the propagation distance is 50000 μm along the MMF fiber section.

of multimode waveguides by which an input field profile is reproduced due to constructive interference to form single or multiple images of the single-mode input field at periodic intervals along the propagation direction of the guide. From Fig. 4, one can see that the first self-imaging distance for the numerical sample of MMF with the refractive index of the cladding layer of $n_{cl} = 1.4271$ is $Z_r = 43010\,\mu$m and a coupling loss to the output SMF fiber of 18.67 dB at a propagation distance of 50 mm. In Fig. 4, due to the cladding refractive index change, the self-imaging distance shifts to the position of $Z_r = 41810\mu$m and the coupling loss is 25.28 dB at a propagation distance of 50 mm. The calculated results show that the eigenmode interference within the MMF section is determined by the refractive index of the cladding layer (in this case, the refractive index of the liquid under test); thus, the transmission loss is affected correspondingly. For a given multimode fiber, i.e., a given refractive index profile, the length of the MMF section is extremely important for defining a one-to-one relationship between the refractive index of the surrounding liquid and the transmission loss within the desired measurable range of the refractive indices. To determine the desirable length of the MMF section, we propose to use the theoretical models presented above to examine the transmission loss as a function of the length of the multimode fiber section and the refractive indices under test. Combining Figs. 3 and 4, the relationship between transmission loss and surrounding refractive index can be obtained. At some propagation positions the transmission loss is relatively sensitive to the MMF length; for example, at propagation distances close to the value of 10 mm, the difference in transmission loss measured at two close propagation distance values of 9.6 and 10.2 mm (also referred to as the discrimination range) is ~20 dB. This suggests that an SMS structure with an MMF length on the order of 10 mm is suitable for refractive index sensing. From the calculated results presented in Fig. 4, it is clear that several possible lengths of the MMF section can be suitable for the refractive index sensing application, such as 10, 20, and 30 mm.

As mentioned above, the refractometer sensor utilizes the multimode interference in the multimode fiber core section, and the surrounding liquid is used as the cladding layer. If the refractive index of the surrounding liquid is higher than the refractive index of the MMF core, the light will leak out instead of providing multimode interference. Therefore, the measurable refractive index should be no higher than that of the MMF core section. Given the core refractive index for the MMF of 1.4446, a desirable measurement range for the refractive index is from 1.33 to 1.44 (the typical refractive indices of liquids are no less than a refractive index value of water, $n_{\text{water}} = 1.33$). As a design example, the range of refractive indices from 1.33 to 1.44 is considered for the refractometer. To determine the exact lengths of the MMF section and a one-to-one relationship between the refractive index of the surrounding liquid and the transmission loss, transmission loss is calculated for refractive indices ranging from 1.33 to 1.44 and for MMF lengths in the regions close to 10, 20, and 30 mm. Corresponding calculated results are presented in Figs. 6(a)–6(c). From Fig. 6 it can be seen that the optimal MMF length should lie in the vicinity of 10, 20, and 30 mm for the required refractive index range. The transmission loss versus refractive index for the corresponding lengths is calculated using the above WABPM models. The one-to-one relationships between the transmission losses and the refractive indices for several selected lengths of MMF are presented in Fig. 7.

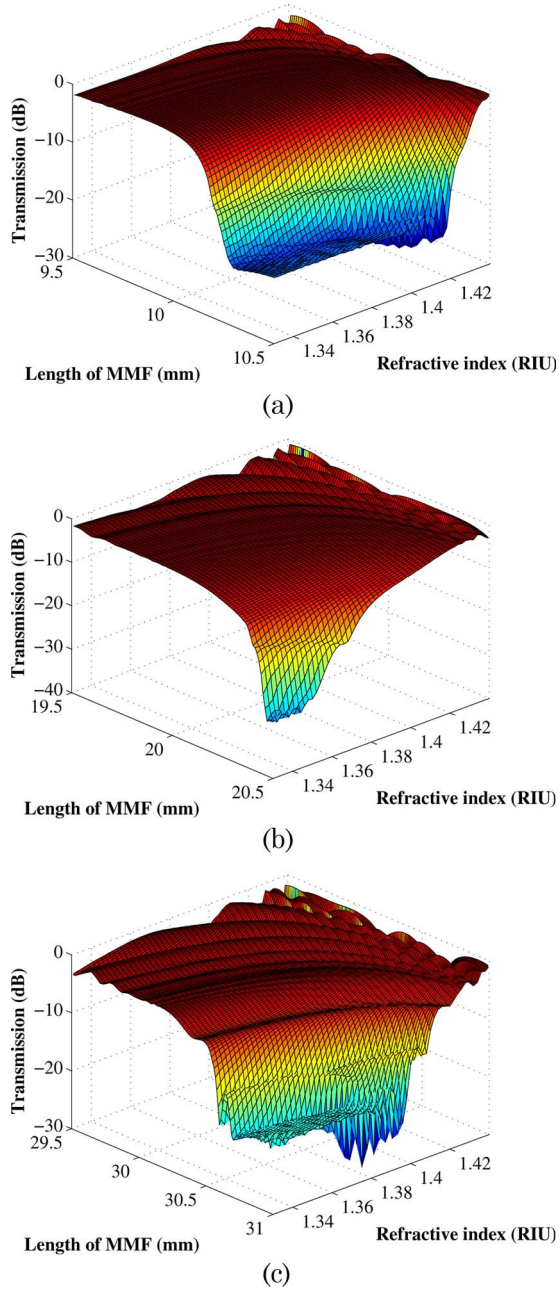

Fig. 6. (Color online) Transmission losses as a function of the length of the MMF section and the refractive indices under test for lengths in the region of (a) 10 mm, (b) 20 mm, and (c) 30 mm.

Figure 7 shows a summary of the relationships between the transmission loss and the refractive index of the surrounding liquid at certain lengths of MMF. As previously mentioned, the eigenmodes of the MMF are determined by the refractive index of the surrounding liquid, which can be treated as a cladding layer, and the multimode interference in the MMF is affected correspondingly. Therefore, the light convergence position along the MMF varies for different surrounding refractive indices, and the structure transmission varies consequently . From Fig. 7, one can also see that there is a

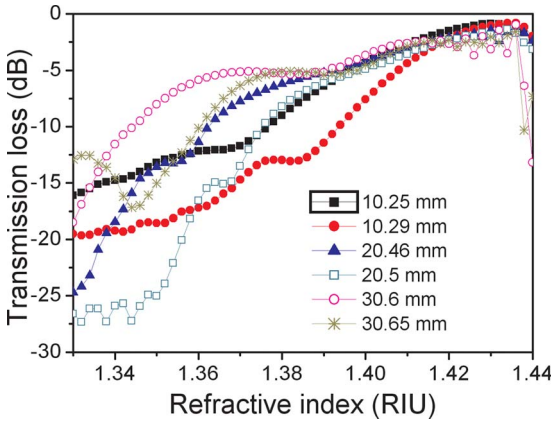

Fig. 7. (Color online) Relationship between transmission loss and refractive index of surrounding liquid for selected MMF lengths.

quasi-linear relationship between the transmission loss and the liquid refractive index when the MMF length lies in the vicinity of 10, 20, and 30 mm. For example, the transmission loss curve for a MMF length of $Z = 10.29$ mm shows a discrimination range from −19.522 dB to −0.916 dB relatively linear over the refractive index range of 1.33–1.432. It is well known that the typical accuracy of commercial optical power meters can be better than 0.01 dB. Therefore, the designed refractometer sensor for $Z = 10.29$ mm has an estimated resolution of 5.48×10^{-5} RIU (refractive index unit). If the desirable measurement range is from 1.333 to 1.382, an estimated resolution of 4.05×10^{-5} is achieved when the length of the MMF is $Z = 30.65$ mm. These results are competitive with those achieved with refractometers based on planar lightwave circuits [9,10].

3. THEORETICAL MODELING AND LIGHT PROPAGATION ANALYSIS IN THE STMS STRUCTURE

A. Proposed STMS Configuration and Its Application for Refractive Index Sensing

From the investigation in Section 2, it is clear that in order to utilize an SMS structure for refractive index sensing, the MMF cladding needs to be removed. The refractive index of the surrounding liquid can then be reliably determined as a function of the transmission loss of the SMS. Experimentally, etching the fiber cladding can be achieved using chemical compounds, such as hydrogen fluoride acid, but this increases the fabrication difficulty and operation risk, and, moreover, the surface roughness induced by chemical etching may lead to a significant discrepancy between the experimental results and theoretical design [11]. Alternatively, an SMS with a tapered structure can be used for the refractive index sensing proposal instead of the chemical etching process. On the other hand, from the investigation above, one can also see that the dynamic range of an SMS-based refractometer is limited to 1.33–1.44 by the refractive index of the MMF fiber core. In practice, a larger dynamic range is desirable for such a refractometer. To achieve a large dynamic range, the cladding layer outside the MMF core is essential and needs to be thin to allow a strong enough power faction propagation in the MMF cladding; the basic principle here is based on the fact that a light wave guided in a fiber has a power faction in the cladding in the form of evanescent wave; the effective index of the cladding modes is determined by the difference between the RI of the cladding and that of the external medium. It is well known that a fiber taper can enhance the fraction of power in the evanescent wave (in the cladding), thus its sensitivity to environmental changes. Since MMFs have a large core diameter and a large numerical aperture, the power in the evanescent field is very small for an untapered MMF; thus, in order to increase it, both the cladding and the core of MMF need to be very thin.

Tapered fibers have attracted considerable interest in recent years owing to both improvements in the taper fabrication technology and the exploitation of tapered fibers in a variety of applications, such as high resolution sensing [12], high-order mode filtering [13], microscopic particle trapping [14], microscale/nanoscale photonic devices [15], and evanescent coupling to planar waveguide or microresonators [16,17]. Tapering can also be an excellent way to thin the fiber cladding layer outside the MMF core. To obtain the desired transmission spectrum without using an extradifficult chemical etching process for a fiber refractometer application, an MMF with a tapered region is investigated below.

The schematic configuration is shown in Fig. 8(a), and corresponding physical parameters of the MMF section are presented in Fig. 8(b).

As a numerical example to illustrate the application of the STMS structure to refractive index sensing, a length of 50 mm of MMF section is chosen. An optical fiber taper is conventionally made by stretching a heated fiber, forming a structure comprising a narrow stretched filament (the taper waist) each end of which is linked to an unstretched fiber by a conical section (the taper transition section), for a fixed heating device with heating zone width L_0 and the same drawing velocity for the two translation stages pulling the fiber to the left and to the right. The length of the taper waist, L_w, corresponds approximately to L_0. In this case, the profile of the taper transition regions is as follows:

$$R(Z) = R_0 \cdot \exp\left(\frac{-Z}{L_0}\right), \tag{11}$$

and the length of each taper transition Z_0 is given by [18]

$$Z_0 = L_0 \cdot \ln\left(\frac{R_0}{R_w}\right), \tag{12}$$

where R_0 is the initial radius of the MMF and R_w is that of the waist radius. From Eqs. (11) and (12), the shape of the taper can be obtained. On the basis of the proposed configuration presented in Fig. 8 and the numerical simulations using the

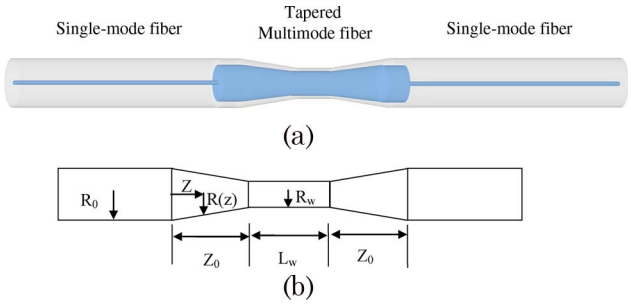

Fig. 8. (Color online) (a) Schematic configuration of the STMS structure; (b) structure of a tapered MMF, illustrating the terminology used in the paper.

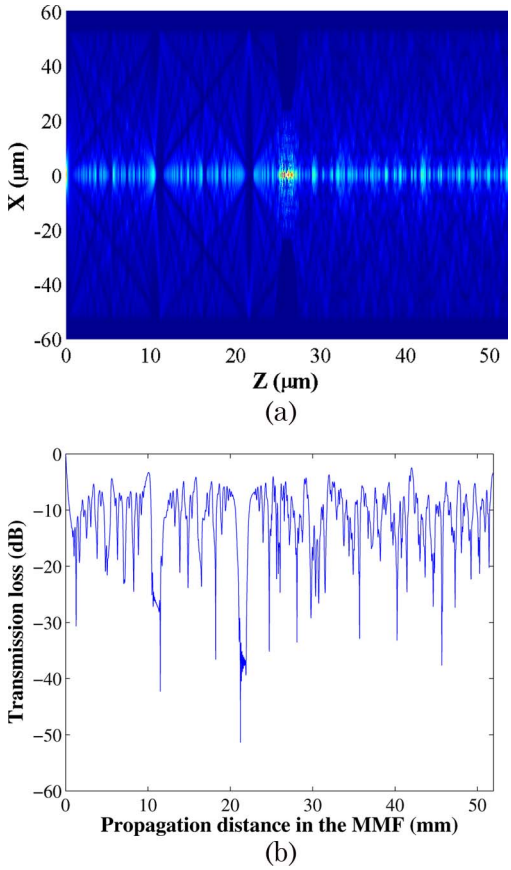

Fig. 9. (Color online) (a) Amplitude distribution of the propagating light, (b) calculated coupling loss to the output SMF fiber as a function of propagation distance.

WABPM mentioned above, the corresponding optical amplitude distributions of the propagation fields and calculated coupling loss to the output of the STMF as a function of propagation distance are presented in Fig. 9. In the theoretical model, the operating wavelength is chosen as 1550 nm, while the length and radius of the core of the tapered MMF are selected as 1 mm and 20 μm, respectively.

From Fig. 9(a), one can see that a few strong mode interference phenomena occur within the tapered MMF section due to the focusing effects of the left tapered transition region. Within the tapered MMF section, the number of modes and the intensity of mode interference within the right tapered section are much smaller and lower than those of the conventional SMS structure, due to the high-order mode filtering effect induced by the tapering [19]. At the same time, a silica cladding layer still exists outside the tapered MMF core between the MMF core and the surrounding liquid; the confinement effect given by this thin cladding layer can expand the dynamic range of this STMS refractometer [20]. In the following investigation, a dynamic range from 1.33 to 1.53 is chosen. The transmission loss versus refractive index is calculated for the entire length of the sandwiched tapered MMF. The unique relationships between the transmission loss and refractive index at two chosen STMS lengths are presented in Fig. 10.

Figure 10 shows that the transmission loss for an MMF tapered length of $Z = 48.5$ mm varies from −13.33 dB to −34.15 dB over the refractive index range of 1.362–1.416 and from −34.15 dB to 10.53 dB over the refractive index range

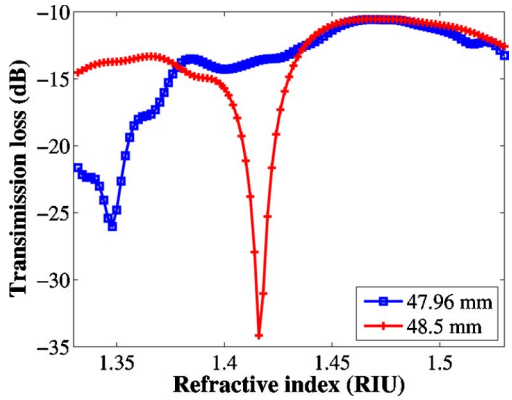

Fig. 10. (Color online) Relationship between transmission loss and refractive index at chosen lengths of tapered MMF.

of 1.416–1.471. The estimated average resolution over the two refractive index ranges is 2.59×10^{-5} and 2.37×10^{-5}, respectively. The measurement dynamic range can be determined by the length of the propagation distance: the STMS with a length of 47.96 mm can offer a wider dynamic range (1.346–1.471) than that of a STMS with a length of 48.5 mm (1.362–1.472). In practice, the results shown in Fig. 10 can be improved, for example, by operating at a different wavelength and by using a tapered MMF with a different length of taper waist, L_w, or a different size of taper radius R_w. Results shown in Fig. 10 also demonstrate feasibility for measuring other analytes, such as gaseous, chemical, or biological analytes, by depositing an appropriate thin sensing layer on the surface of the tapered region of the MMF.

4. CONCLUSION

In conclusion, light propagation within SMS and STMS fiber structures has been investigated using the WABPM with a Padé (3, 3) approximate operator and PML boundary conditions. The application of two such fiber structures as refractometer sensors for measuring the unknown refractive index of a liquid sample has been numerically demonstrated. A Thorlabs AFS105/125Y step index multimode fiber has been employed in the models for practical use. The effect of strong mode interference on the device's performance has been studied and demonstrated numerically. Results indicate that the STMS structure allows for measurement of refractive indices in a much wider refractive index range with a reasonably high resolution. Although only a refractometric sensor is considered in this paper, the proposed STMS device can also be optimized and developed further as an edge filter, which is widely used in optical communications or optical fiber sensing systems. Moreover, by further optimizing a number of physical parameters for the proposed fiber device (such as the lengths and shapes of both down- and up-tapers, the length and radius of the tapered waist segment, the thickness of the cladding layer, and the position of the tapered section within the MMF), a more compact fiber sensing device with an improved performance can be realized. Investigation of an optimal design and associated experimental fabrication of such a sensor will be carried out in the near future.

ACKNOWLEDGMENTS

P. Wang is funded by the Irish Research Council for Science, Engineering and Technology, cofunded by the Marie-Curie

Actions under FP7. G. Brambilla gratefully acknowledges the Royal Society (London) for his research fellowship, Q. Wu gratefully acknowledges the support of Science Foundation Ireland under grant 07/SK/I1200.

REFERENCES

1. A. Mehta, W. S. Mohammed, and E. G. Johnson, "Multimode interference-based fiber optic displacement sensor," IEEE Photon. Technol. Lett. **15**, 1129–1131 (2003).
2. W. S. Mohammed, A. Mehta, and E. G. Johnson, "Wavelength tunable fiber lens based on multimode interference," J. Lightwave Technol. **22**, 469–477 (2004).
3. Q. Wang and G. Farrell, "All-fiber multimode-interference based refractometer sensor: proposal and design," Opt. Lett. **31**, 317–319 (2006).
4. W. S. Mohammed, P. W. E. Smith, and X. Gu, "All-fiberr multimode interference bandpass filter," Opt. Lett. **31**, 2547–2549 (2006).
5. G. R. Hadley, "Wide-angle beam propagation using Padé approximant operators," Opt. Lett. **17**, 1426–1428 (1992).
6. W. Press, B. Flannery, S. Teukolsky, and W. Vetterling, *Numerical Recipes: the Art of Scientific Computing* (Cambridge University, 1990).
7. G. R. Hadley, "Multistep method for wide-angle beam propagation," Opt. Lett. **17**, 1743–1745 (1992).
8. L. B. Soldano and E. C. M. Pennings, "Optical multimode interference devices based on self-imaging: principles and applications," J. Lightwave Technol. **13**, 615–627 (1995).
9. R. Bernini, S. Campopiano, C. de Boer, P. M. Sarro, and L. Zeni, "Planar antiresonant reflecting optical waveguides as integrated optical refractometer," IEEE Sens. J. **3**, 652–657 (2003).
10. G. J. Veldhuis, L. E. W. van der Veen, and P. V. Lambeck, "Integrated optical refractometer based on waveguide bend loss," J. Lightwave Technol. **17**, 857–864 (1999).
11. P. Wang, Y. Semenova, Q. Wu, G. Farrell, Y. Ti, and J. Zheng, "Macrobending single-mode-fiber-based refractometer," Appl. Opt. **48**, 6044–6049 (2009).
12. R. K. Verma, A. K. Sharma, and B. D. Gupta, "Surface plasmon resonance based tapered fiber optic sensor with different taper profiles," Opt. Commun. **281**, 1486–1491 (2008).
13. Y. Jung, G. Brambilla, and D. J. Richardson, "Comparative study of the effective single-mode operational bandwidth in subwavelength optical wires and conventional single-mode fibers," Opt. Express **17**, 16619–16624 (2009).
14. Z. Liu, C. Guo, J. Yang, and L. Yuan, "Tapered fiber optical tweezers for microscopic particle trapping: fabrication and application," Opt. Express **14**, 12510–12516 (2006).
15. G. Brambilla, "Optical fiber nanowires and microwires: a review," J. Opt. **12**, 043001 (2010).
16. R. Sarkissian, S. Farrell, and J. D. O'Brien, "Spectroscopy of a tapered-fiber photonic crystal waveguide coupler," Opt. Express **17**, 10738–10747 (2009).
17. Frank Vollmer and Stephen Arnold, "Whispering-gallery-mode biosensing: label-free detection down to single molecules," Nat. Methods **5**, 591–596 (2008).
18. T. A. Birks and Y. W. Li, "The shape of fiber tapers," J. Lightwave Technol. **10**, 432–438 (1992).
19. Denis Đonlagić, "Inline higher order mode filters based on long highly uniform fiber tapers," J. Lightwave Technol. **24**, 3532–3539 (2006).
20. Joel Villatoro, David Monzón-Hernández, and Donato Luna-Moreno, "Inline optical fiber sensors based on cladded multimode tapered fibers," Appl. Opt. **43**, 5933–5938 (2004).